Robust s_{±} pairing in CaK(Fe_{1−x}Ni_{x})_{4}As_{4} (x=0 and 0.05) from the response to electron irradiation

S. Teknowijoyo, K. Cho, M. Kończykowski, E. I. Timmons, M. A. Tanatar, W. R. Meier, M. Xu, S. L. Bud'ko, P. C. Canfield, and R. Prozorov

Phys. Rev. B **97**, 140508 — Published 27 April 2018

DOI: 10.1103/PhysRevB.97.140508

Robust $s_\pm$ pairing in CaK$(Fe_{1-x}Ni_x)_4As_4$ ($x = 0$ and 0.05) from the response to electron irradiation

S. Teknowijoyo,[1,2] K. Cho,[1,2] M. Kończykowski,[3] E. I. Timmons,[1,2] M. A. Tanatar,[1,2] W. R. Meier,[1,2] M. Xu,[1,2] S. L. Bud'ko,[1,2] P. C. Canfield,[1,2] and R. Prozorov[1,2,*]

[1] *Ames Laboratory, Ames, IA 50011*

[2] *Department of Physics & Astronomy, Iowa State University, Ames, IA 50011*

[3] *Laboratoire des Solides Irradiés, École Polytechnique, CNRS, CEA, Université Paris-Saclay, 91128 - Palaiseau Cedex, France*

(Dated: Submitted: 15 February 2018; Revised: 14 April 2018)

Controlled point-like disorder introduced by 2.5 MeV electron irradiation was used to probe the superconducting state of single crystals of CaK$(Fe_{1-x}Ni_x)_4As_4$ superconductor at $x = 0$ and 0.05 doping levels. Both compositions show an increase of the residual resistivity and a decrease of the superconducting transition temperature, T_c, at the rate of $dT_c/d\rho(T_c) \approx 0.19$ K/($\mu\Omega$·cm) for x =0 and 0.38 K/($\mu\Omega$·cm) for x =0.05, respectively. In the Ni-doped compound ($x = 0.05$), the coexisting spin-vortex crystal (SVC) magnetic phase is suppressed at the rate of $dT_N/d\rho(T_N) \approx 0.16$ K/($\mu\Omega$·cm). The low-temperature variation of London penetration depth is well approximated by the power law function, $\Delta\lambda(T) = AT^n$, with $n \approx 2.5$ for $x = 0$ and $n \approx 1.9$ for $x = 0.05$ in the pristine state. Detailed analysis of $\lambda(T)$ and T_c evolution with disorder is consistent with two effective nodeless energy gaps in the density of states due to robust $s_\pm$ pairing. Overall the behavior of CaK$(Fe_{1-x}Ni_x)_4As_4$ at $x = 0$ is similar to a slightly overdoped $Ba_{1-y}K_yFe_2As_2$ at $y \approx 0.5$, and at $x = 0.05$ to an underdoped composition at $y \approx 0.2$.

INTRODUCTION

The hole-doped iron-based superconductor, $Ba_{1-y}K_yFe_2As_2$ (BaK122), has a complex temperature-doping phase diagram [1]. In the parent compound, $BaFe_2As_2$, stripe-type magnetic order sets in at the Néel temperature, T_N, simultaneously with the tetragonal to orthorhombic structural transition at T_s [2]. Upon K-doping, the magnetic order is suppressed and superconductivity appears at about $y \approx 0.18$. Coexistence of stripe magnetic order and superconductivity in the underdoped regime ($y \leq 0.24$) [3] leads to substantial anisotropy of the superconducting gap [4], rapidly increasing in the underdoped compositions. These observations suggest that the interplay of superconductivity and magnetism may be of importance for the superconducting pairing, in line with theoretical suggestions [5–7].

The discovery of stoichiometric $CaKFe_4As_4$ (CaK1144) [8–10] provided unique opportunity to study effectively hole-doped system without additional scattering from chemically substituted ions. In terms of electron count, $CaKFe_4As_4$ corresponds to $Ba_{1-y}K_yFe_2As_2$ at $y = 0.5$, and, indeed, their properties are very similar [9, 11], but with a notably lower residual resistivity in CaK1144 due to the absence of substitution-induced disorders. London penetration depth [11, 12] and STM [11, 13] studies of the $CaKFe_4As_4$ are consistent with the two effective gaps Δ_1 and Δ_2 in the range of 6-10 meV and 1-4 meV, respectively, which is close to the behavior found near $y = 0.5$ composition of $Ba_{1-y}K_yFe_2As_2$ [14]. Electron-doping of $CaKFe_4As_4$ with Ni and Co leads to a magnetic order, similar to the underdoped composition with $y \leq 0.25$ of $Ba_{1-y}K_yFe_2As_2$, albeit of a different type, which is the spin-vortex crystal (SVC) magnetic order [15]. In view of clear effect of magnetism on superconducting gap anisotropy in $Ba_{1-y}K_yFe_2As_2$ [4, 16] it is of interest if change from stripe spin density wave (SSDW) to SVC magnetic structure would affect superconductivity.

In this work, we study the superconducting gap structure of $CaKFe_4As_4$ in both stoichiometric and Ni-doped samples with different amount of point-like disorder. This controlled disorder is characterized by measuring normal state resistivity as described elsewhere [17]. The effect on the superconducting state is revealed by measuring the changes in T_c and low-temperature variation of London penetration depth $\Delta\lambda(T)$. We find nodeless superconducting gaps, along with a rapid suppression of T_c with disorder, a strong indication for $s_\pm$ pairing [18]. We do not find any obvious effect of the SVC type of magnetic ordering on superconductivity in Ni-doped compound.

EXPERIMENT

Single crystals of CaK$(Fe_{1-x}Ni_x)_4As_4$ ($x = 0$ and 0.05) were grown from a high temperature solution rich in Fe and As [9, 10]. The composition of Ni-doped crystals was determined by electron probe microanalysis with wavelength dispersion spectroscopy. Detailed description of crystal synthesis and characterization using X-ray difraction, magnetization, heat capacity and resistivity are reported elsewhere [9, 15]. Since microscopic inclusions of superconducting impurity phases below X-ray diffraction resolution are frequently observed in $CaKFe_4As_4$ crys-

tals [9, 10], samples for penetration depth and resistivity measurements were screened using custom made sensitive radio-frequency susceptometer [19]. Only samples with sharp transitions and no additional features on temperature scans were selected. In the end, a pair of samples selected for high-resolution penetration depth measurement had typical dimensions of $0.5 \times 0.5 \times 0.02$ mm^3. Samples for resistivity measurements were shaped into bars with dimensions about $0.7 \times 0.2 \times 0.02$ mm^3. Electrical contacts to the samples were made by soldering silver wires using tin [20, 21]. The contacts were sufficiently mechanically stable to survive irradiation, so that the same samples were measured before and after irradiation, thus enabling quantitative comparison without invoking uncertainty of geometric factor determination. Four-probe electrical resistivity was measured in *Quantum Design* PPMS.

A self-oscillating tunnel-diode resonator (TDR) technique was used for in-plane London penetration depth measurements. The samples were placed into a 40 turns inductor coil, which is a part of an LC tank circuit. The sample and the coil were thermally decoupled, and the temperature of the circuit and coil was actively stabilized around 5 K with sub-mK accuracy. The change in the resonant frequency shift due to temperature-dependent screening of small, ∼20 mOe, excitation AC magnetic field into the sample was calibrated by determining the sample geometry and measuring frequency change when the sample is physically removed from the coil at the base temperature (∼ 450 mK). Detailed description of the technique and calibration can be found elsewhere [22–24]. Dedicated crystals for penetration depth study were also measured before and after irradiation, which are separate from the set of crystals for resistivity.

Electron irradiation was performed at SIRIUS Pelletron linear accelerator in Laboratoire des Solides Irradiés at École Polytechnique in Palaiseau, France. The irradiation was conducted using 2.5 MeV electrons in liquid hydrogen environment at ∼ 22 K to provide efficient heat dissipation and prevent immediate recombination of the vacancy-interstitial defects (Frenkel pairs). Upon warming to room temperature after irradiation, about 20 to 30 percent of defects are annealed as indicated by the decrease of the residual resistivity measured *in-situ* [17]. After this initial annealing, the defects remain relatively stable as long as the samples are kept at room temperature. We re-measured several $Ba_{1-y}K_yFe_2As_2$ samples near optimal doping after months of passive storage in a desiccator at room temperature and did not detect significant changes [14]. We plan to perform similar measurements on the CaKNi1144 samples used in this study. On the other hand, some fraction of the remaining defects can be annealed by deliberately warming samples above the room temperature. When a sample was warmed up to 400 K, T_c was increased (Fig. 2 (a)). The defect concentration produced by electron irradiation in the MeV range is homogeneous throughout the sample due to the large penetration depth (∼ 100 µm) of MeV range electrons [25]. This can be seen directly from the fact that the transitions remain sharp after irradiation. The acquired irradiation dose presented in this paper is in the units of coulomb per square centimeter, where 1 C/cm^2 = 6.24 x 10^{18} electrons/cm^2. The total charge of electrons penetrated through the sample was measured by the Faraday cage behind the sample stage.

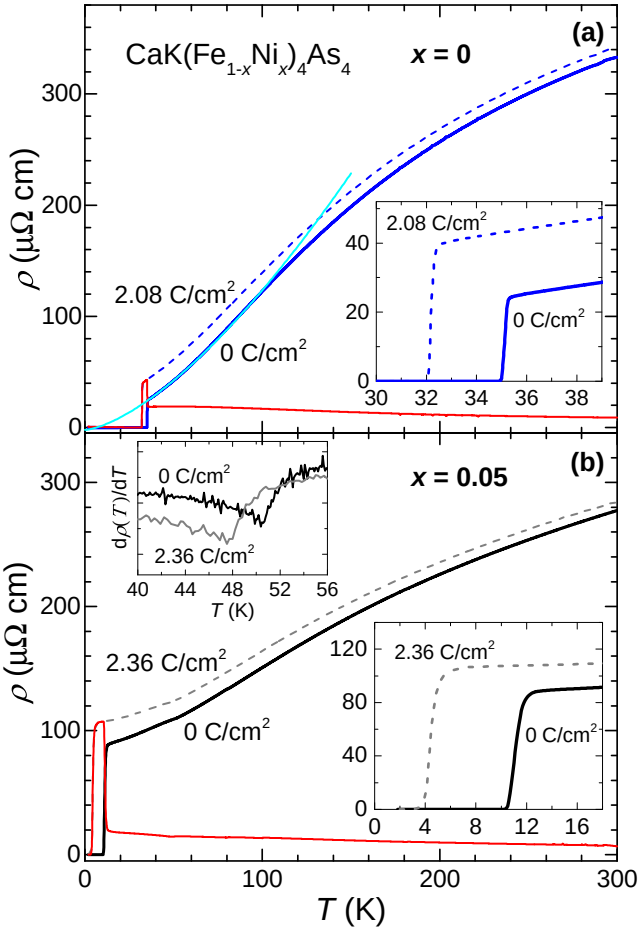

FIG. 1. **(Color online)** In-plane resistivity of stoichiometric $CaKFe_4As_4$ sample ($x = 0$, top panel **(a)**) and Ni-substituted sample ($x = 0.05$, bottom panel **(b)**). Solid and dashed lines show resistivity of the samples before and after irradiation, with doses 2.08 C/cm^2 ($x = 0$) and 2.38 C/cm^2 ($x = 0.05$). Red lines show the change of resistivity between irradiated and pristine states. Cyan line in the top panel is fit of the curve in pristine $x = 0$ sample to $\rho(0) + \rho_T T^{3/2}$. Right insets zoom on the superconducting transition range. Left inset in the bottom panel shows temperature-dependent resistivity derivative zooming on the features at T_N, suppressed upon irradiation from 50.6 K to 47.5 K.

RESULTS AND DISCUSSION

Figure 1 shows in-plane resistivity of the parent $CaKFe_4As_4$ (top panel) and Ni-doped $CaK(Fe_{0.95}Ni_{0.05})_4As_4$ (bottom panel) before (solid lines) and after (dashed lines) electron irradiation with 2.08 C/cm^2 and 2.38 C/cm^2, respectively. In-plane resistivity of $x = 0$ sample in pristine state shows cross-over feature at about 200 K, typical for all hole-doped compositions. Approaching T_c on cooling, $\rho(T)$ shows small upward curvature, similar to $Ba_{1-y}K_yFe_2As_2$ where it can be fitted with $\sim T^{3/2}$ dependence in a limited temperature range from 40 K to 60 K [26]. Similar power law fits the data well in $CaKFe_4As_4$ as shown in the top panel of Fig. 1 (cyan line). The resistivity just above the onset of resistive transition is about 12 times lower than ρ(300K). The actual residual resistivity is impossible to extrapolate convincingly, since $T^{3/2}$ fit gives small negative value of $\rho(0)$ and T_c is large. The resistive transition to the superconducting state at T_c(onset) = 35.2 K is very sharp (see lower inset in top panel of Fig. 1) with width of $\Delta T_c < 0.5$ K, reflecting good sample quality. Electron irradiation of 2.08 C/cm^2 leads to a vertical shift of the $\rho(T)$ curve, with red line in top panel of Fig. 1 showing the difference between $\rho(T)$ curves before and after irradiation. The shift is not constant, its value just above T_c is about two times higher than at room temperature, suggesting violation of the Matthiessen rule. The superconducting transition remains sharp after the irradiation supporting homogeneous defect distribution. The suppression of T_c with increase of residual resistivity $\rho(T_c)$, happens at a rate, $dT_c/d\rho(T_c)$ = -0.19 K(μΩcm)$^{-1}$, which is remarkably close to that of slightly over-doped $Ba_{1-y}K_yFe_2As_2$ (see Fig. 3(a) below for direct comparison).

The electrical resistivity $\rho(T)$ of Ni - doped sample, $x = 0.05$, in the pristine condition is shown by a solid curve in the bottom panel of Fig. 1. It has similar broad cross-over feature at 200 K, though it is much less pronounced due to significant increase of residual resistivity compared to pure $x = 0$ compound ($\approx$ 100 μΩcm, lower inset in Fig. 1(b)). An additional feature in $\rho(T)$ curves of $x = 0.05$ sample can be distinguished in the temperature-dependent resistivity derivative at ~50 K (top inset in Fig. 1(b)), most likely due to spin-vortex crystal (so-called "hedgehog") magnetic ordering [15]. Electron irradiation with total dose of 2.38 C/cm^2 with subsequent annealing at room temperature (dashed curve in Fig. 1(b)) leads to an upward shift of the $\rho(T)$ curve. Similar to the pristine sample, the shift is temperature dependent and is significantly bigger for $T < T_N \sim 47$ K suggesting partial loss of the carrier density. The magnetic transition temperature is suppressed from 50.6 K to 47.5 K, while the superconducting transition temperature is suppressed from 10.5 to 4 K (lower inset in Fig. 1(b)).

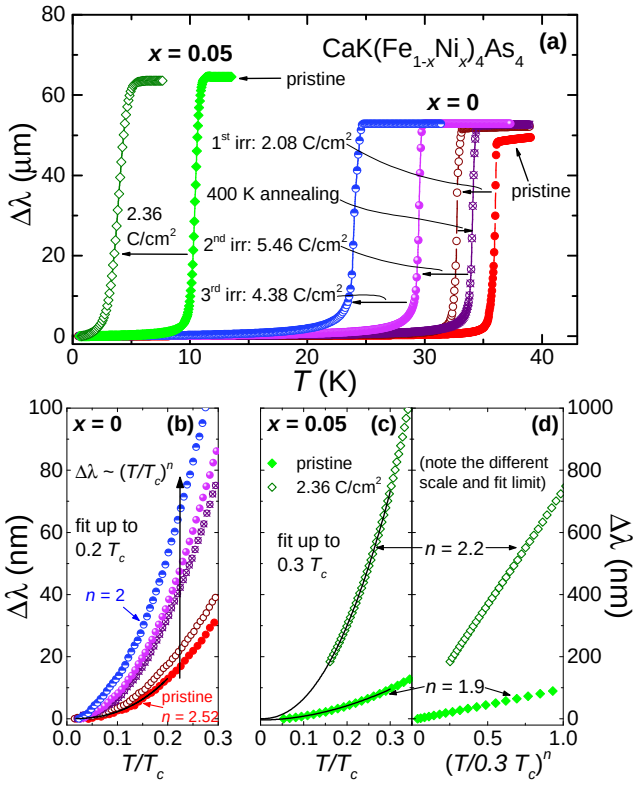

FIG. 2. **(Color online) (a)** Full temperature range $\Delta\lambda(T)$. For the stoichiometric ($x = 0$) sample the data were taken in a sequence of irradiation / annealing treatments as indicated in the legend. **(b)** Low temperature part of $\Delta\lambda(T/T_c)$ in $x = 0$ sample. The exponent n monotonically decreases with irradiation/annealing treatments in a sequence specified in top panel. Two right bottom panels show $\Delta\lambda$ in Ni-doped sample $x = 0.05$ plotted as a function of T/T_c (panel **(c)**) and of $(T/T_c)^n$ (panel **(d)**).

The rate of T_c suppression with increase of residual resistivity is substantially higher than in the sample with $x = 0$ (see Fig. 3(a)). Rapid suppression of both superconducting and magnetic transition temperatures with irradiation is very similar to underdoped BaK122 [27] where superconductivity also coexists with magnetism, albeit with a different antiferromagnetic structure (stripe - type).

To probe the superconducting state, London penetration depth measurement on a pair of samples was done before and after irradiation. This pair is different from the pair used exclusively for the transport study. While only single irradiation dose of 2.36 C/cm^2 was applied to a Ni - doped ($x = 0.05$) sample, multiple irradiations with intermediate annealing to 400 K were performed on pure ($x = 0$) sample. Top panel of Fig. 2 shows total variation $\Delta\lambda(T)$ over the whole superconducting range from the base temperature of 0.4 K to above superconducting T_c for both samples. For x =0 sample, the superconducting transition temperature, T_c, was suppressed by

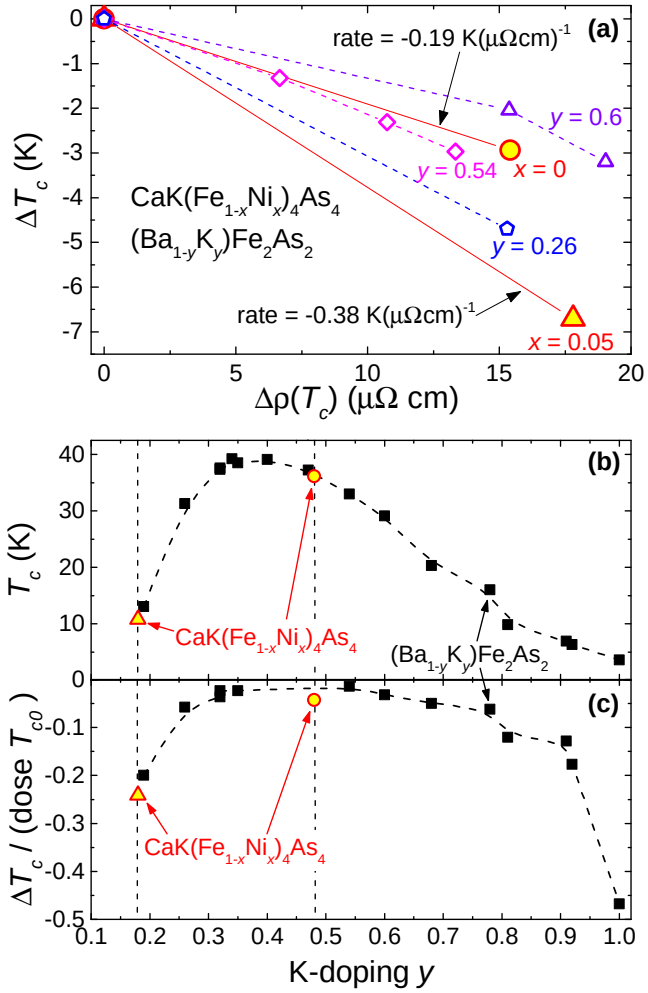

FIG. 3. **(Color online) (a)** T_c suppression with irradiation parameterized via change in resistivity, $\Delta\rho(T_c)$. The rate of T_c suppression in stoichiometric $CaKFe_4As_4$ ($x = 0$) is similar to nearly optimally doped $Ba_{1-y}K_yFe_2As_2$ $y = 0.54$ and 0.6 [11]. Ni - doped ($x = 0.05$) sample is close to underdoped $Ba_{1-y}K_yFe_2As_2 y = 0.26$. **(b)** and **(c)** Summary of T_c suppression normalized by the irradiation dose and T_{c0} as a function of potassium doping y, where $CaKFe_4As_4$ compounds are placed in $y = 0.18$ and 0.48 following the T_c "dome" of $Ba_{1-y}K_yFe_2As_2$. T_c values are taken from Refs. [14, 27].

3.2 K from $T_c^{pristine}$(onset) = 36.1 K after first dose of 2.08 C/cm^2, partially recovered by 1.3 K after 400 K annealing, and then further decreased by 9.7 K after second 5.46 C/cm^2 and third 4.38 C/cm^2 irradiations, so in the end T_c^{final} = 24.5 K. The sample in the pristine state (red curve) has the lowest residual resistivity resulting a small value of skin-depth, so the total rf field penetration above T_c is determined by the skin depth. However, the skin depth gets larger than sample size for doped and irradiated samples due to the increase of residual resistivity, so the total rf field penetration depth above T_c is determined by the sample size. The change in total penetration depth above T_c is shown in Fig. 2(a).

The bottom panels of Fig. 2 zoom on the low-temperature part of the $\Delta\lambda(T/T_c)$. The range $T/T_c < 0.3$ is considered "low - temperatures", where the superconducting gap can be considered as practically temperature-independent and thermally excited quasiparticles reflect the gap topology in the reciprocal space. The panel (b) shows data for $x = 0$ sample after multiple irradiations. The panels (c) and (d) show data for sample $x = 0.05$ plotted against reduced temperature T/T_c and $(T/T_c)^n$ scales, respectively. Although the annealing process slightly reversed the trend of T_c evolution in $x = 0$ case, the low temperature features, namely the absolute variation of the penetration depth $\Delta\lambda(T) = \lambda(T) - \lambda(T_{min})$ and the exponent n of the power law fit $\Delta\lambda(T) = AT^n$ both exhibit monotonic behavior (see Fig. 2 (b)). The total variation of the London penetration depth below $T/T_c = 0.3$ is proportional to the amount of thermally excited quasiparticles [28], while the exponent n is a measure of pair - breaking scattering and superconducting energy gap anisotropy. Monotonic evolution of $\Delta\lambda(0.3T_c)$ as opposed to non-monotonic evolution of T_c suggests that even though the defects (mostly Frenkel pairs) partially recombine during annealing to give way to higher T_c, there are residual low energy pair-breaking states in the underlying gap structure that are not recovered by the annealing. The exponent n in $x = 0$ sample gradually decreases from $n = 2.5$ (pristine) to $n = 2$, as expected for superconductors without nodes in the gap approaching the dirty limit [24], indicating the s_{++} or $s_{\pm}$ gap structures as potential candidates. However, strong T_c suppression favors $s_{\pm}$ pairing, similar to the scenario discussed in other reports [11–13].

The data of Fig. 2(b) indicate that disorder is more efficient pairbreaker in the Ni - doped sample x =0.05 compared to the undoped counterpart $x = 0$, as seen in notably higher total variation of the penetration depth between base temperature and $T/T_c = 0.3$ and larger fractional T_c suppression. Application of the power law fit for a temperature range from base temperature up to 0.3 T_c (black lines, Fig. 2(c)) for x =0.05 yields $n = 1.9$, which slightly increased to 2.2 after irradiation of 2.36 C/cm^2. By plotting $\Delta\lambda(T)$ vs T^n, we verify the quality of the fit. It is easy to notice notable increase of the prefactor A after irradiation, reflecting increased quasiparticle density [28]. The slight increase of the exponent to above $n = 2$ suggests that in pristine state, $x = 0.05$ sample is not yet in the regime where impurity scattering dominates (dirty limit) where exponent should saturate at $n = 2$ with increasing disorder [29]. Rather, in light of previous study in underdoped $Ba_{1-y}K_yFe_2As_2$ in which long range magnetism gives rise to gap anisotropy [4, 30], the increase of exponent is consistent with the averaging of the gap structure causing the gap become more isotropic and minima to be elevated. An alternative explanation could invoke $c-$axis point node [24] suggested for electron-doped $Ba(Fe_{1-x}Co_x)_2As_2$ from anisotropic

thermal conductivity [31, 32] and $c-$axis penetration depth [33] measurements. However, this scenario does not have any current theoretical or $k-$resolved spectroscopic support and, therefore, is unlikely.

At this point, it is clear that the behavior of $CaK(Fe_{1-x}Ni_x)_4As_4$ with $x = 0$ (x =0.05) projects nicely on $Ba_{1-y}K_yFe_2As_2$ system at $y \approx 0.5$ ($y \approx 0.2$). Parallels drawn in the text show good matching in T_c suppression rate with irradiation and the evolution of low-temperature London penetration depth variation along with the exponents of the power-law analysis. Finally, it is possible to fit $CaK(Fe_{1-x}Ni_x)_4As_4$ into $Ba_{1-y}K_yFe_2As_2$ the phase diagram, which is best illustrated in Fig. 3 (b) and (c), where the comparison to $Ba_{1-y}K_yFe_2As_2$ compounds is presented by plotting T_c, and its sensitivity to disorder, as function of potassium doping. In Fig. 3 (b), following $Ba_{1-y}K_yFe_2As_2$ "dome", stoichiometric $CaKFe_4As_4$ can be placed in the vicinity of optimal and slightly overdoped region ($y = 0.48$), whereas electron doped $CaK(Fe_{0.95}Ni_{0.05})_4As_4$ can be positioned on the underdoped side ($y = 0.18$) where superconductivity and magnetism coexist. Figure 3 (c) shows suppression of T_c normalized by the irradiation dose and T_{c0} which serves as experimental measure of the sensitivity to scattering and allows comparison between different materials. Compared to BaK122, pure $CaKFe_4As_4$ seems to be somewhat more sensitive to disorder but $CaK(Fe_{0.95}Ni_{0.05})_4As_4$ actually matches very nicely. These observations are naturally explained by the fact that pristine CaK1144 ($x = 0$) is cleaner than BaK122 ($y \approx 0.5$), so the effect of additional disorder is more pronounced. In the doped system, on the other hand, substitution disorder is similar between the two systems. It is rather remarkable that such good mapping is possible in similar, but still different and complex materials. Considered together, presented results make very strong case for robust and ubiquitous $s_\pm$ pairing in iron based superconductors.

CONCLUSIONS

Electron irradiation with 2.5 MeV electrons results in a rapid suppression of the superconducting transition temperature, T_c, in both stoichiometric $CaKFe_4As_4$ and spin vortex crystal (SVC) antiferromagnetic Ni-doped $CaKFe_4As_4$, $x = 0.05$, suggesting sign changing superconducting energy gap. In both cases the low-temperature variation of London penetration depth is consistent with nodeless superconducting state. The two observations provide strongest support for $s_\pm$ pairing in these multiband superconductors. Detailed analysis shows remarkable similarity between $CaKFe_4As_4$ compositions at $x = 0$ and $x = 0.05$ with hole-doped $Ba_{1-y}K_yFe_2As_2$ at $y \approx 0.5$ and $y \approx 0.2$, respectively, despite the difference in the spin structure in the magnetically ordered state.

ACKNOWLEDGEMENT

This work was supported by the U.S. Department of Energy (DOE), Office of Science, Basic Energy Sciences, Materials Science and Engineering Division. Ames Laboratory is operated for the U.S. DOE by Iowa State University under contract DE-AC02-07CH11358. WRM was supported by the Gordon and Betty Moore Foundations EPiQS Initiative through Grant GBMF4411. We thank the SIRIUS team, B. Boizot, V. Metayer, and J. Losco, and especially O. Cavani, for running electron irradiation at Ecole Polytechnique (supported by EMIR network, proposal 15-5788).

* Corresponding author: prozorov@ameslab.gov

[1] M. Rotter, M. Tegel, and D. Johrendt, Phys. Rev. Lett. **101**, 107006 (2008).
[2] P. C. Canfield and S. L. Bud'ko, Annual Review of Condensed Matter Physics **1**, 27 (2010).
[3] S. Avci, O. Chmaissem, D. Y. Chung, S. Rosenkranz, E. A. Goremychkin, J. P. Castellan, I. S. Todorov, J. A. Schlueter, H. Claus, A. Daoud-Aladine, D. D. Khalyavin, M. G. Kanatzidis, and R. Osborn, Phys. Rev. B **85**, 184507 (2012).
[4] H. Kim, M. A. Tanatar, W. E. Straszheim, K. Cho, J. Murphy, N. Spyrison, J.-P. Reid, B. Shen, H.-H. Wen, R. M. Fernandes, and R. Prozorov, Phys. Rev. B **90**, 014517 (2014).
[5] D. Parker, M. G. Vavilov, A. V. Chubukov, and I. I. Mazin, Phys. Rev. B **80**, 100508 (2009).
[6] J.-P. Ismer, I. Eremin, E. Rossi, D. K. Morr, and G. Blumberg, Phys. Rev. Lett. **105**, 037003 (2010).
[7] R. M. Fernandes and J. Schmalian, Phys. Rev. B **82**, 014521 (2010).
[8] A. Iyo, K. Kawashima, T. Kinjo, T. Nishio, S. Ishida, H. Fujihisa, Y. Gotoh, K. Kihou, H. Eisaki, and Y. Yoshida, Journal of the American Chemical Society **138**, 3410 (2016).
[9] W. R. Meier, T. Kong, U. S. Kaluarachchi, V. Taufour, N. H. Jo, G. Drachuck, A. E. Böhmer, S. M. Saunders, A. Sapkota, A. Kreyssig, M. A. Tanatar, R. Prozorov, A. I. Goldman, F. F. Balakirev, A. Gurevich, S. L. Bud'ko, and P. C. Canfield, Phys. Rev. B **94**, 064501 (2016).
[10] W. R. Meier, T. Kong, S. L. Bud'ko, and P. C. Canfield, Phys. Rev. Materials **1**, 013401 (2017).
[11] K. Cho, A. Fente, S. Teknowijoyo, M. A. Tanatar, K. R. Joshi, N. M. Nusran, T. Kong, W. R. Meier, U. Kaluarachchi, I. Guillamón, H. Suderow, S. L. Bud'ko, P. C. Canfield, and R. Prozorov, Phys. Rev. B **95**, 100502 (2017).
[12] P. K. Biswas, A. Iyo, Y. Yoshida, H. Eisaki, K. Kawashima, and A. D. Hillier, PHYSICAL REVIEW B **95** (2017).

[13] A. Fente, W. R. Meier, T. Kong, V. G. Kogan, S. L. Bud'ko, P. C. Canfield, I. Guillamon, and H. Suderow, (2016).

[14] K. Cho, M. Kończykowski, S. Teknowijoyo, M. A. Tanatar, Y. Liu, T. A. Lograsso, W. E. Straszheim, V. Mishra, S. Maiti, P. J. Hirschfeld, and R. Prozorov, Science Advances **2** (2016).

[15] W. R. Meier, Q.-P. Ding, A. Kreyssig, S. L. Bud'ko, A. Sapkota, K. Kothapalli, V. Borisov, R. Valentí, C. D. Batista, P. P. Orth, R. M. Fernandes, A. I. Goldman, Y. Furukawa, A. E. Böhmer, and P. C. Canfield, npj Quantum Materials **3**, 5 (2018).

[16] J.-P. Reid, M. A. Tanatar, X. G. Luo, H. Shakeripour, S. R. de Cotret, A. Juneau-Fecteau, J. Chang, B. Shen, H.-H. Wen, H. Kim, R. Prozorov, N. Doiron-Leyraud, and L. Taillefer, Phys. Rev. B **93**, 214519 (2016).

[17] R. Prozorov, M. Kończykowski, M. A. Tanatar, A. Thaler, S. L. Bud'ko, P. C. Canfield, V. Mishra, and P. J. Hirschfeld, Phys. Rev. X **4**, 041032 (2014).

[18] I. I. Mazin, D. J. Singh, M. D. Johannes, and M. H. Du, Phys. Rev. Lett. **101**, 057003 (2008).

[19] M. A. Tanatar, W. E. Straszheim, H. Kim, J. Murphy, N. Spyrison, E. C. Blomberg, K. Cho, J.-P. Reid, B. Shen, L. Taillefer, H.-H. Wen, and R. Prozorov, Phys. Rev. B **89**, 144514 (2014).

[20] M. A. Tanatar, N. Ni, S. L. Budko, P. C. Canfield, and R. Prozorov, Superconductor Science and Technology **23**, 054002 (2010).

[21] M. A. Tanatar, R. Prozorov, N. Ni, S. L. Bud'ko, and P. C. Canfield, U.S. Patent No. **8,450,246** (2011).

[22] R. Prozorov, R. W. Giannetta, A. Carrington, and F. M. Araujo-Moreira, Phys. Rev. B **62**, 115 (2000).

[23] R. Prozorov and R. W. Giannetta, Superconductor Science and Technology **19**, R41 (2006).

[24] R. Prozorov and V. G. Kogan, Reports on Progress in Physics **74**, 124505 (2011).

[25] M. W. Thompson, *Defects and Radiation Damage in Metals, p. 142, by M. W. Thompson, Cambridge, UK: Cambridge University Press* (1974).

[26] Y. Liu, M. A. Tanatar, W. E. Straszheim, B. Jensen, K. W. Dennis, R. W. McCallum, V. G. Kogan, R. Prozorov, and T. A. Lograsso, Phys. Rev. B **89**, 134504 (2014).

[27] K. Cho, M. Kończykowski, J. Murphy, H. Kim, M. A. Tanatar, W. E. Straszheim, B. Shen, H. H. Wen, and R. Prozorov, Phys. Rev. B **90**, 104514 (2014).

[28] K. Hashimoto, K. Cho, T. Shibauchi, S. Kasahara, Y. Mizukami, R. Katsumata, Y. Tsuruhara, T. Terashima, H. Ikeda, M. A. Tanatar, H. Kitano, N. Salovich, R. W. Giannetta, P. Walmsley, A. Carrington, R. Prozorov, and Y. Matsuda, Science **336**, 1554 (2012).

[29] M. M. Korshunov, Y. N. Togushova, and O. V. Dolgov, Physics-Uspekhi **59**, 1211 (2017).

[30] S. Maiti, R. M. Fernandes, and A. V. Chubukov, Phys. Rev. B **85**, 144527 (2012).

[31] M. A. Tanatar, J.-P. Reid, H. Shakeripour, X. G. Luo, N. Doiron-Leyraud, N. Ni, S. L. Bud'ko, P. C. Canfield, R. Prozorov, and L. Taillefer, Phys. Rev. Lett. **104**, 067002 (2010).

[32] J.-P. Reid, M. A. Tanatar, X. G. Luo, H. Shakeripour, N. Doiron-Leyraud, N. Ni, S. L. Bud'ko, P. C. Canfield, R. Prozorov, and L. Taillefer, Phys. Rev. B **82**, 064501 (2010).

[33] C. Martin, H. Kim, R. T. Gordon, N. Ni, V. G. Kogan, S. L. Bud'ko, P. C. Canfield, M. A. Tanatar, and R. Prozorov, Phys. Rev. B **81**, 060505 (2010).